On The Collapse of a Gas Cavity by an Imploding Molten Lead Shell and Richtmyer-Meshkov Instability

Victoria Suponitsky, Sandra Barsky, and Aaron Froese

General Fusion Inc., 108-3680 Bonneville Place, Burnaby, BC V3N 4T5,Canada

Email: *victoria.suponitsky@generalfusion.com*

1 ABSTRACT

With an eye to investigating the collapse of a spherical gas cavity, we examine the propagation of a pressure pulse in molten lead, *Pb* in 1, 2 and 3 dimensions, using the open source CFD software OpenFOAM. Results are compared to the theoretical predictions of the collapse of a bubble. We investigate the Richtmyer-Meshkov instability[1, 2] in cylindrical geometry, at Atwood number $A = -1$ for a number of different initial perturbations and pressure pulses.

2 INTRODUCTION

In this paper we consider the collapse of a gas cavity by an imploding molten lead (*Pb*) shell. This process can be accompanied by development of Richtmyer-Meshkov instability [1, 2](RMI). Our interest lies in Magnetized Target Fusion, and in particular, in the factors relevant to the compression of a gas cavity by liquid lead. A scale model of this system is currently under construction at General Fusion Inc. In our prototype model a cylindrical or spherical imploding pressure wave, created by pneumatic pistons, travels through the molten lead and strikes the interface between the *Pb* and a gas. The gases of interest include air, argon and plasma. The interface undergoes a rapid acceleration and travels toward the center, compressing the gas. Disturbances existing at the interface prior to the passage of the pressure wave may seed development of hydrodynamic instabilities at later stages. Therefore, the estimation of the disturbances' growth rates and an exploration of the parameters affecting this growth are of great importance with regard to the initially required smoothness of the interface for efficient compression. This work primarily aims to deepen our understanding of the entire collapse process including hydrodynamic instabilities which may influence the efficiency of the target compression in Magnetized Target Fusion. A secondary goal is to understand the limitations of our current numerical capabilities and to pave the way for improvements in the future.

When a pressure wave hits an interface separating two fluids, there is both a transmitted and reflected wave. The ratio between the latter waves depends on the ratio of acoustic impedances, $Z = \rho c$, of each fluid, where ρ and c are the density and sound speed respectively. For our experiment, the reflected wave is a rarefaction wave[3]. If the interface has perturbations, the development of the Richtmyer-Meshkov instability[1, 2] (RMI) may occur.

The vast majority of work concerning RMI has been done in a planar geometry and a number of models describing linear as well as nonlinear stages of the perturbation growth have been developed [4, 5]. There has been recent interest focused on RMI in convergent geometries [6, 7, 8, 9, 10]. Pressure pulses in convergent geometries are more complicated than in the planar case. The convergence itself leads to acceleration and amplification of the pulse, regardless of any instabilities. Furthermore there are secondary effects such as reshock, which further complicate the scenario. A full understanding of RMI in cylindrical or spherical geometry has yet to be achieved.

This article is organized as follows: the numerical method and setup are described in §3. Results of the cylindrical and spherical collapse of unperturbed cavity are given §4.1 and the results concerning RMI in cylindrical geometry are presented in §4.2.

3 NUMERICAL METHOD AND SETUP

Simulations were performed using the open source CFD code OpenFOAM [11]. The compressible multiphase solver 'compressibleInterFoam' was used in these simulations. This solver implements the Volume Fraction (VoF) method for interface tracking and

is suitable for the simulation of two compressible immiscible isothermal fluids. A barotropic equation of state is implemented in the solver to close the system of continuity and momentum equations. For each of the phases it is given by:

$$\rho_i = \rho_0 + \psi_i P \tag{1}$$

where $\psi = 1/c^2$ is the compressibility and c is the speed of sound. For a compressible phase the nominal density ρ_0 is set to zero. This results in an ideal gas equation of state for isothermal flow. For an incompressible phase, i.e. liquid, ρ_0 is set to a nominal density of the liquid under the normal conditions; the fluid density then remains essentially constant unless the liquid is subjected to the very high pressures. The majority of the simulations were carried out in a

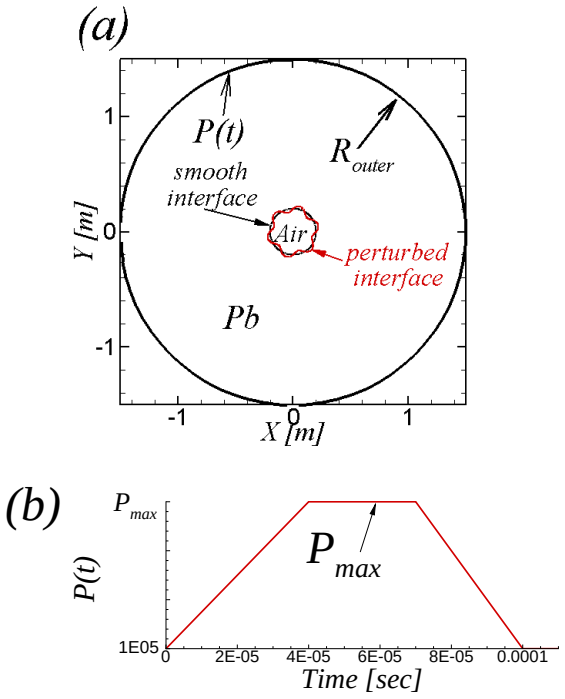

Figure 1: (a) Numerical setup for 2D simulations in a cylindrical geometry; (b) Shape of the pressure pulse imposed on the outer boundary.

2D cylindrical geometry. The outer radius was set to $R_{outer} = 1.5m$, and the initial interface was located at $R_{interface} = 0.2m$. A very small central part with radius $r < 0.01m$ has not been solved to avoid unnecessarily small time steps due to the very small size of the grid cells in this region. The effect of 'taking out' the centre was found to be negligible for the purposes of this work. A cylindrical mesh with $n_r = 2800$ and $n_\theta = 800$ grid points in the radial and azimuthal directions, respectively, was used in the simulations. At the outer boundary, R_{outer}, a pressure pulse was imposed as time-dependent boundary condition $P(t)$. In most cases a pulse duration was $T_{pulse} \approx 1 \times 10^{-4}s$, which is approximately what we expect in our scale model. At the inner boundary $R_{inner} = 0.01m$ a zero gradient boundary condition for both pressure and velocity was prescribed. Initially both fluids were in rest and at atmospheric pressure.

Simulations were carried out for both smooth and sinusoidally perturbed interfaces. The former is mainly for the validation purposes and the latter for studying potential development of instabilities due to the initial imperfection of the interface. A schematic of the setup and shape of the pressure pulse are shown in Figs. 1(a) and (b), respectively. A 3D spherical implosion was also simulated in the case of a smooth interface. For such simulations a 20^o degree spherical segment was used as a computational domain with periodic boundary conditions applied on either side of the segment. In the radial (r) and azimuthal (θ) directions the number of grid points was reduced by factor of two compared to the 2D cylindrical mesh and in the periodic direction (ϕ) $n_\phi = 23$ points was used.

For a perturbed interface, the initial sinusoidal perturbation, defined by its initial amplitude A and azimuthal wave number n, was imposed in the beginning of the simulation. The initial amplitude was defined relative to the radial location of the unperturbed interface as:

$$A_{perturbation} = \frac{r_{max} - R_{interface}}{R_{interface}} \times 100\%, \tag{2}$$

and the azimuthal mode n is given by $n = 2\pi R_{interface}/\lambda$, where λ is the perturbation wavelength.

All but one of the simulations were carried out for an implosion from molten lead, Pb, into air. One simulation for an implosion from Pb into water was performed for comparison. The densities and sound speeds are: Pb $\rho_1 = 10000kg/m^3$, $c_1 = 2000m/s$; air $\rho_2 = 1kg/m^3$, $c_2 = 316m/s$; water $\rho_{water} = 1000kg/m^3$, $c_{water} = 1500m/s$. The Atwood number for these simulations is $A = (\rho_2 - \rho_1)/(\rho_2 + \rho_1) = -1$ for Pb-air, and $A = -0.81$ for Pb-water.

4 Results

4.1 Pulse propagation and gas cavity collapse: unperturbed interface

In this section we present results for the pressure pulse propagation through the Pb in convergent geometry and a subsequent collapse of the air cavity with an initially unperturbed interface. The results are compared with existing theoretical solutions. A summary

of the relevant processes affecting the pressure pulse is (i) amplification of the pressure, due to the convergent geometry and steepening of the pressure pulse during its propagation through the *Pb*; (ii) nearly complete reflectance of the pressure pulse back into the lead. The reflected wave is a rarefaction wave that subjects the molten lead to tension which in turn causes cavitation; (iii) when the *Pb*/air interface is hit by the pulse, the interface undergoes a rapid acceleration and continues its movement toward the center, compressing the air. A *Pb* shell converges towards center, and is separated from the rest of the lead by the cavitation region.

Pressure pulse propagation through the *Pb* for cylindrical and spherical geometries are shown Figs. 2 (a) and (b), respectively. Results are shown for two amplitudes of the pulse: $P_1 = P_{max} = 1.5 \times 10^8 Pa$ and $P_2 = P_{max} = 1.5 \times 10^9 Pa$. These amplitudes correspond to the pressures attainable in our scale model. A relation between particle velocity, V_p, and the pressure of the pulse is given by:

$$V_p = \frac{P_{max} - P_o}{\rho_1 c_1} \approx \frac{P_{max}}{\rho_1 c_1}. \qquad (3)$$

Eq. 3 leads to the initial particle velocities of $V_p \approx 7.5 m/s$ and $V_p \approx 75 m/s$ for pulses P_1 and P_2, respectively. Linear behaviour is expected for P_1 whereas P_2 might exhibit non-linearities. Fig. 2 demonstrates the following: (i) the amplification of the pressure pulse during its propagation through *Pb* is in excellent agreement with theoretical predictions [12]; $P \sim 1/\sqrt{r}$ for cylindrical and $P \sim 1/r$ for spherical geometries; (ii) the steepening of the pulse due to the nonlinear effects, and (iii) the time taken for the pulse to propagate from the outer boundary to the interface is $t_{propagation} = 6.5 \times 10^{-4} s$, which agrees with the prescribed speed of sound $c_1 = 2000 m/s$.

VoF contours at the time the pressure pulse hits the interface and later during the collapse are shown in Figs. 3(a) and (b) for the pulse P_2 in cylindrical geometry. This figure clearly demonstrates the formation of the *Pb* shell moving toward the center and the formation of a cavitation region behind the shell separating it from the rest of the molten lead. Fig. 4 shows radial profiles of the pressure, velocity and VoF during the collapse. Results are presented for cylindrical geometry and pressure pulse P_1. VoF profiles clearly show the location of the interface, the formation and growth of the cavitation region once the interface starts moving towards the center and also the increase of the *Pb* shell thickness during the collapse process. From the pressure profiles we can see the pressure build up inside the *Pb* shell, the sudden drop of the pressure in the cavitation region and increase of the pressure inside the air

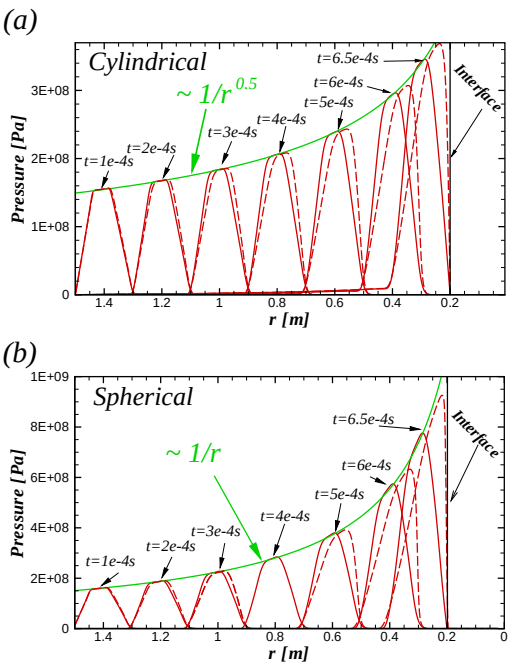

Figure 2: Pressure pulse propagation from the outer boundary at $r = 1.5m$ towards the interface at $r = 0.2m$ in (a) cylindrical and (b) spherical geometry. Solid and broken lines correspond to the pulse amplitudes of $P_{max} = 1.5 \times 10^8 Pa$ and $P_{max} = 1.5 \times 10^9 Pa$, respectively. The pulse propagates from the left to the right.

as it is getting compressed. Several important features of the flow field can be observed. Firstly, when the pulse reaches the interface (Fig. 4a), the particle velocity and pressure are in a good agreement with Eq. 3 especially if the slight increase in lead density is taken into account. Secondly, once the interface starts moving, its velocity which is equal to the fluid velocity at the position of the interface, roughly corresponds to

$$V_{interface} \approx 2 \times V_p, \qquad (4)$$

where V_p is given by Eq. 3 with P_{max} taken as a maximum pressure of the pulse just before it hits the interface. This is in agreement for expected result of two fluids with large impedance ratio (§4.8 and §4.9 in [13]). Thirdly, there is a gradual increase in velocity in the cavitation region followed by further increase inside the *Pb* shell. Lastly, a shock wave is generated inside the air as a result of the sudden acceleration of the interface. This acceleration of the interface can be viewed as an analogy to a piston starting from the rest and suddenly moving with constant velocity into a quiescent gas. In this situation, a shock front immediately appears, moving away from the piston with a constant and supersonic speed. Ahead of the shock front the

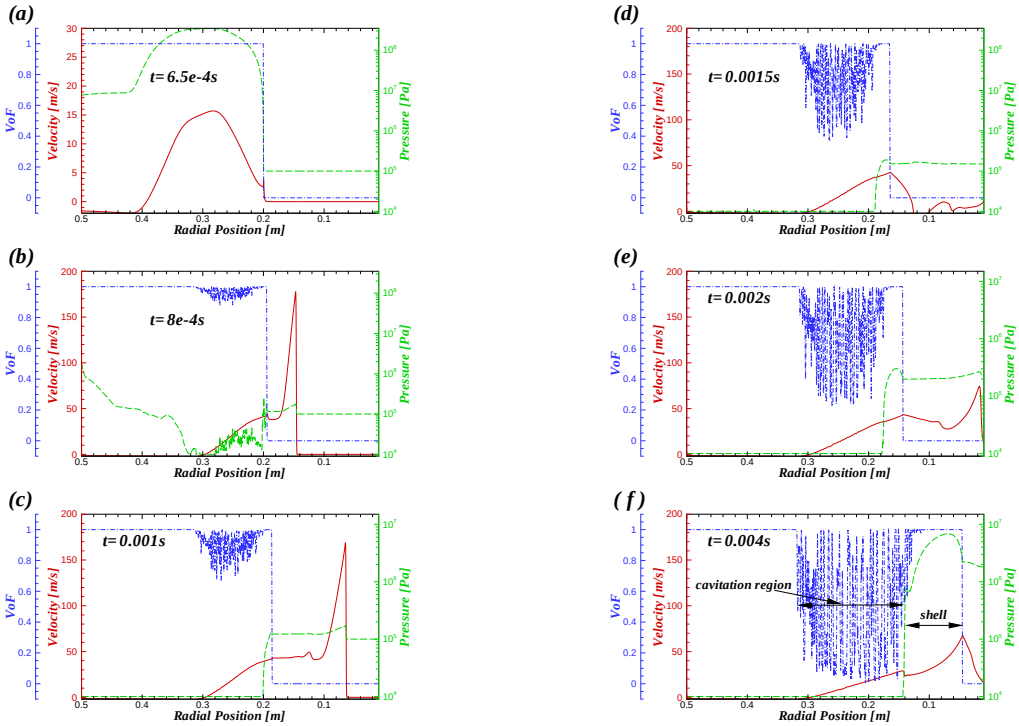

Figure 4: This figure illustrates the radial profiles of: the pressure, broken green line; velocity, solid red line; and VoF, dash-dot blue line at and after the pulse hits the interface for cylindrical geometry, $P_{max} = 1.5 \times 10^8 Pa$.

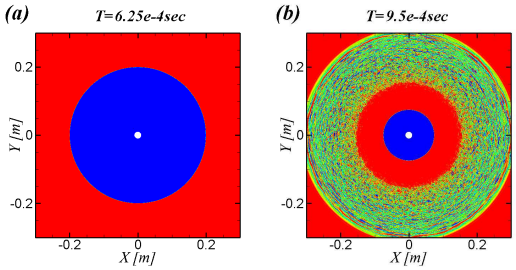

Figure 3: VoF contours at (a) $T = 6.5 \times 10^{-4}$sec, pulse hits the interface, and (b) $T = 9.5 \times 10^{-4}$sec, during the cavity collapse. Cylindrical geometry, $P_{max} = 1.5 \times 10^9 Pa$.

gas is at rest, while behind the shock it moves with the velocity equal to that of the piston, i.e. the interface velocity in our case (see [14] §3). It is worth noting that while the shock inside the air is an important feature of the flow field, it has little effect on the *Pb* shell evolution and therefore it is not the focus of our work.

A correct prediction of the gas cavity collapse is necessary for the reliable estimation of the compression efficiency in our system and also for further studies of potential instabilities. Fig. 5(a) shows the interface position during the collapse for all geometries for the low amplitude pulse, P_1. We compare our results to a semi-analytical solution of Kedrinskii (§ 1.4 in [15]), Fig. 5. The agreement is excellent for a $1D$ cartesian case and at early times for cylindrical and spherical geometries. The main reason for the disparity between our results and Kedrinskii's [15] is the finite duration of the pressure pulse in our simulations. By increasing the duration of the pulse the differences between our results and Kedrinskii are considerably reduced. It is also worth noting that our current simulations allow the air to escape the computational domain resulting in a complete collapse of the cavity. Thus, in our case the interface is accelerated during the entire collapse. In reality, however, the interface will undergo deceleration during the latest stages of compression because of the high gas pressure. This deceleration might be important for the potential development of the Rayleigh-Taylor instability, but it is not our current focus.

It is also worth noting that while the acoustic pressure pulse hits the interface at the same time of $T = 6.5 \times 10^- 4s$ regardless of its initial amplitude and geometry, the initial interface velocity and, consequently, the collapse time, are proportional to the pulse amplitude at the time it hits the interface. Therefore, the results for different geometries and initial pulse ampli-

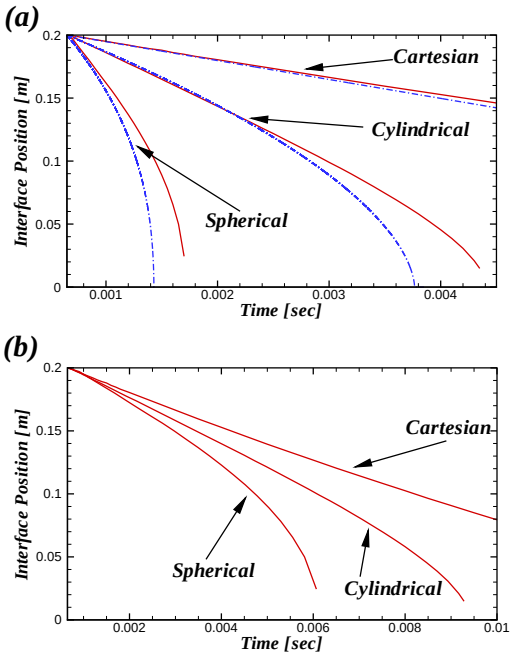

Figure 5: Interface position during the cavity collapse for cartesian, cylindrical and spherical geometries for the pulse with $P_{max} = 1.5 \times 10^8 Pa$. (a) OpenFoam: red solid line; Kedrinskii (§1.4 in [15]) analytical solution: blue dash-dot line. (b) OpenFOAM results for the case where the pulse amplitude is the same for all geometries when the pulse hits the interface at $T = 6.5 \times 10^{-4} s$ and equal to $P = 1.5 \times 10^8 Pa$.

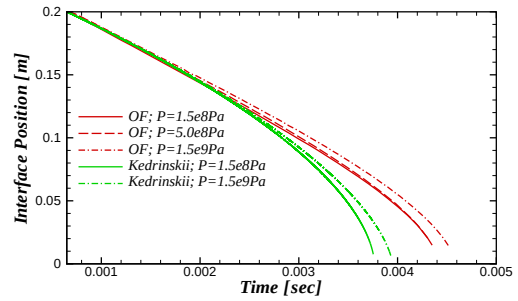

Figure 6: Effect of the pressure pulse amplitude on the collapse of the gas cavity. Results are shown for cylindrical geometry and scaled for comparison with low amplitude pulse with $P_{max} = 1.5 \times 10^8 Pa$.

tudes can be scaled such that the initial interface velocity is the same. This is presented in Fig. 5(b) where the same results shown in Fig. 5(a) are scaled to P_1.

Finally the effect of the initial pulse amplitude on the collapse time is shown in Fig. 6 for the cylindrical geometry. The results are scaled so that the initial interface velocity corresponds to P_1. It can be seen that OpenFOAM results are identical for pulses with $P_{max} = 1.5 \times 10^8 Pa$ and $P_{max} = 5 \times 10^8 Pa$ indicating that at these amplitudes non-linear effects are insignificant. Results also show that for high amplitude pulses, P_2, the nonlinearity begins to manifest by increasing the time of collapse due to the energy losses. Deviations from the linear pulse are very similar for OpenFOAM and Kedrinskii [15] results.

4.2 RM-Instability

We now turn our attention to the development of RMI during the gas cavity collapse as a result of an initial imperfection of the interface. Effects of initial perturbation amplitude, azimuthal wave-number and pressure pulse amplitude are addressed.

The effect of the initial perturbation amplitude on the evolution of the perturbation during the collapse is shown in Fig. 7 by VoF contours. Simulations were performed for four different amplitudes (Eq. 2): (i) $A_1 = 0.5\%$; (ii) $A_2 = 2.5\%$; (iii) $A_3 = 5\%$ and $A_4 = 15\%$ for the perturbation with azimuthal wave-number $n = 6$ and pressure pulse P_2. One can see that after the pressure pulse strikes the interface the characteristic pattern of RMI, namely a mushroom of light fluid penetrating into heavy fluid and vice versa, starts to develop. The finger of light fluid poking into the heavy fluid is usually called a bubble, and that of the heavy into the light is called a spike. If the shock starts in the heavy fluid the sinusoidal perturbation initially flattens, and then inversion occurs [6]. During inversion, what had been a finger of light fluid penetrating into the heavy becomes a finger of heavy fluid penetrating into the light fluid. In the present case of a very large ratio of fluid densities, the spikes are significantly sharper when compared with those at lower Atwood numbers. This has been also observed by Tian *et al.* [8]. It can be also seen that shape of the molten lead shell and cavitation region are affected by the initial imperfection of the interface.

The time evolution of the amplitudes of the spikes and bubbles at different initial perturbation amplitudes is plotted in Fig. 8. The amplitude of the spikes and bubbles are calculated as their radial position minus the position of undisturbed interface. We also show the average perturbation amplitude which is calculated

as $(r_{max} - r_{min})/2$. For a very small amplitude of $A_1 = 0.5\%$ (Fig. 8a) the perturbation evolution can be described as linear during the entire collapse because the growth rates of spikes and bubbles are almost symmetrical. Also the perturbation growth does not seem to slow down during the collapse. With increasing amplitude, nonlinear effects become obvious, as can be seen in Fig. 8(b),(c) and (d). A dominant nonlinear effect is the increasing disparity of growth rates between spikes and bubbles: spikes appear to accelerate once the inversion has occurred, i.e. they grow faster than linear scaling with amplitude would imply, while the bubble growth is slower than linear scaling. This can be also observed by the increase in deviation of average perturbation amplitude from that of spike with the increase in initial perturbation amplitude. Fig. 9 shows an alternative representation of the results where the time evolution of spikes and bubbles is shown by their radial position. The position of the undisturbed interface for comparison.

The effect of the azimuthal wave-number on the perturbation growth is shown in Fig. 10 for the perturbation with initial amplitude of $A_3 = 5\%$ and pressure pulse P_2. This figure clearly demonstrates that the disparity in the growth of spikes and bubbles increases with an increase in azimuthal wave-number. It also seems that even at initial stages, before inversion, the growth rates do not really scale with wave-mode number. A close-up of the perturbation structure at late stages of the collapse for the different azimuthal modes is shown in Fig. 11 by the VoF contours. It can be observed that for higher azimuthal modes a secondary Kelvin-Helmholtz instability starts to develop on the sides of the spike because of the strong velocity shear.

For the sake of completeness the perturbation evolution for the pulses of different strength, P_1 and P_2 are shown in Figs. 12(a) and (b), respectively, for the perturbation with amplitude $A_{max} = 5\%$ and azimuthal mode $n = 6$. Fig. 12(a) shows radial position of the spike, bubbles and the unperturbed interface, and Fig. 12(b) shows the amplitude of spike and bubbles relative to the undisturbed interface. The results for a weaker pulse are scaled with the amplitude ratio of the pressure pulses for the comparison; the curves do not collapse, indicating the lack of a linear relation.

Finally, for comparison, we show some results of implosion of molten lead into water. The equation of state used for water is Eq. 1 with appropriate values for ρ_o and c, i.e. both fluids are basically incompressible. The Atwood number is $A = -0.81$ and ratio of acoustic impedances is $Z_1/Z_2 = 13.3$. In this case the disturbance evolution is considerably different from that discussed earlier. Since the water can hardly be compressed, the interface moves only bit toward the center before it springs back. Phase inversion occurs, however, the spike penetration is not as dramatic as before. Also no cavitation has been observed in the case. Fig. 13 illustrates the perturbation evolution in this case.

REFERENCES

[1] R.D. Richtmyer. Taylor instability in shock acceleration of compressible fluids. *Commun. Pure Appl. Math.*, 13:297-319, 1960.

[2] E.E. Meshkov. Instability of the interface of two gases accelerated by a shock wave. *Fluid Dyn.*, 4(5):101-104, 1969.

[3] Y. Yang and Q. Zhang and D.H. Sharp. Small amplitude theory of Richtmyer-Meshkov Instability. *Phys. Fluids*, 6:1856-873, 1993.

[4] M. Latini and O. Schilling and W.S. Don. High-resolution simulations and modeling of reshocked single-mode Rychtmyer-Meshkov instability: Comparison to experimental data and to amplitude growth model predictions. *Phys. Fluids*, 19:024104, 2007.

[5] M. Brouillette The Richtmyer-Meshkov Instability. *Annu. Rev. Fluid Mech*, 34:445-68, 2002.

[6] Q. Zhang and M.J. Graham A numerical study of Richtmyer-Meshkov instability driven by cylindrical shocks. *Phys. Fluids*, 10:974–992, 1998.

[7] J.R. Fincke, N.E. Lanier, S.H.Batha, R.M. Hueckstaedt, G.R. Magelssen, S.D. Rothman, K.W. Parker and C.J.Horsfield. Postponement of Saturation of the Richtmyer-Meshkov Instability in a Convergent Geometry. *Phys. Rev. Letters*, 93(11):115003, 2004.

[8] B. Tian and D. Fu and Y. Ma. Numerical investigation of Richtmyer-Meshkov instability driven by cylindrical shocks. *Acta Mech Sinica*, 22:9–16, 2006.

[9] M. Lombardini and D.I. Pullin. Small-amplitude perturbations in the three-dimensional cylindrical Richtmyer-Meshkov instability. *Phys. Fluids*, 21:114103, 2009.

[10] R. Krechetnikov. Rayleigh-Taylor and Richtmyer-Meshkov instabilities of flat and curved interfaces. *J. Fluid Mech.*, 625:387, 2009.

[11] OpenFOAM. www.openfoam.org.

[12] Landau L. D. and Lifshitz E. M. Fluid Mechanics (2nd Ed.). *Pergamon Press*, 1987.

[13] Thompson, P. A. Compressible-Fluid Dynamics. *Maple Press Company*, 1984.

[14] R. Courant and K. O. Friedrichs. Supersonic Flow and Shock Waves. *Springer-Verlag*, 1976.

[15] V. K. Kedrinskii. Hydrodynamics of Explosion. *Springer-Verlag*, 2005.

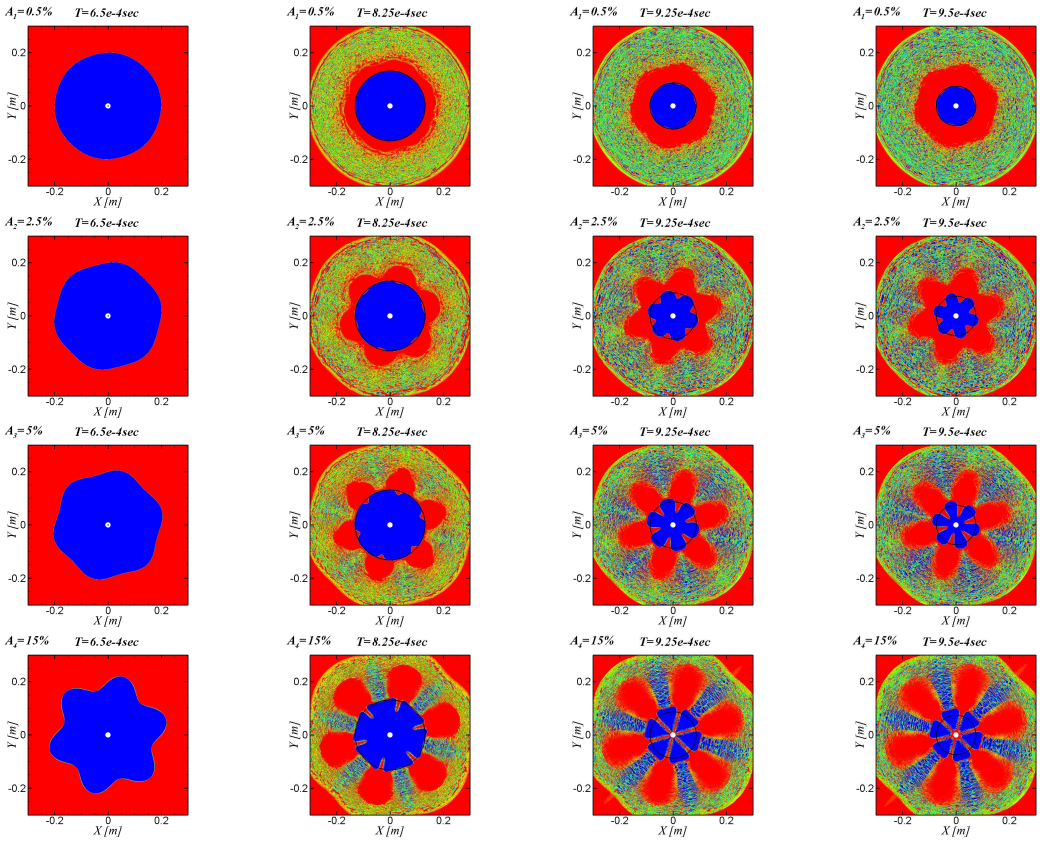

Figure 7: Effect of the initial perturbation amplitude shown by the VoF contours. Red is the *Pb*, blue is the gas, and the mixed colours indicate the cavitation regime. Perturbation is $n = 6$, and the pressure pulse amplitude is $P_{max} = 1.5 \times 10^9 Pa$. Black circles correspond to the interface position for the unperturbed case.

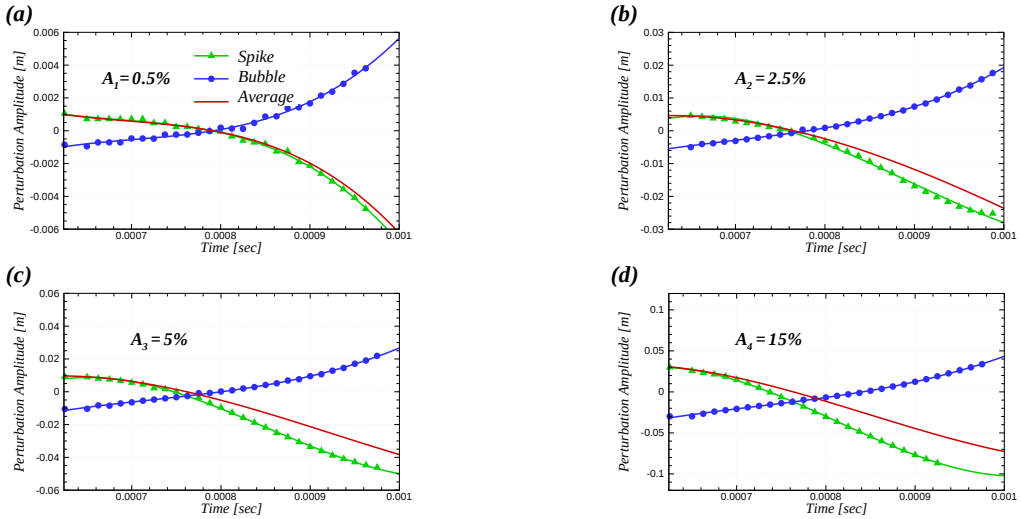

Figure 8: Effect of the perturbation amplitude: green and blues lines - amplitude of the spikes and bubbles relative to the unperturbed interface; red lines - averaged amplitude calculated as $(r_{max} - r_{min})/2$. Perturbation is at azimuthal mode of $n = 6$, and the pressure pulse amplitude is $P_{max} = 1.5 \times 10^9 Pa$.

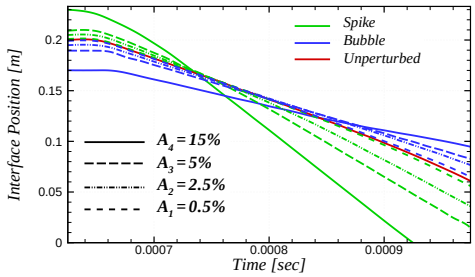

Figure 9: Radial location of spikes and bubbles (green and blue lines) for different amplitudes of the initial perturbation. Interface location for the unperturbed case (red line) is also shown. Results are for a pulse with $P_{max} = 1.5 \times 10^9$ Pa and a perturbation with azimuthal mode of $n = 6$.

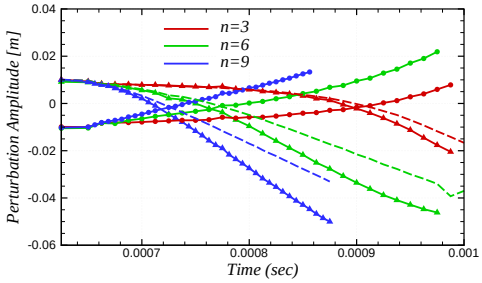

Figure 10: Effect of azimuthal mode number: Amplitude of spikes and bubbles relative to the position of the unperturbed interface for perturbations with $n = 3$ (red lines), $n = 6$ (green lines) and $n = 9$ (blue lines). Results are shown for the perturbation with initial amplitude of $A_3 = 5\%$ and pulse with $P_{max} = 1.5 \times 10^9 Pa$.

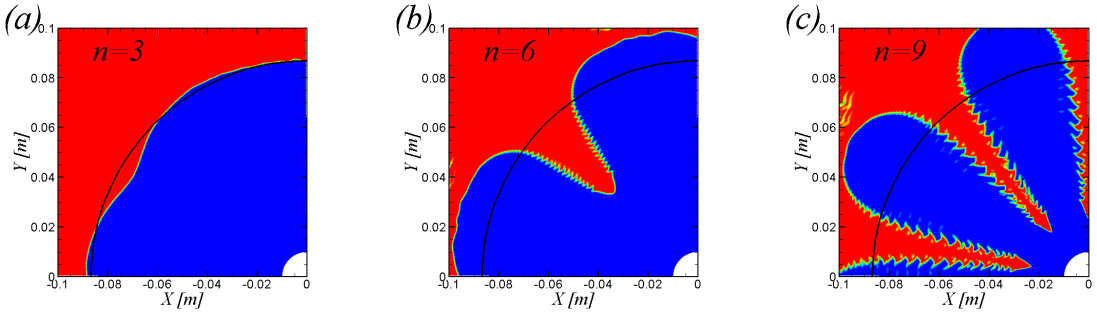

Figure 11: Close-up look on the perturbation structure during the collapse ($T = 9.25 \times 10^{-4} sec$) at different azimuthal modes. Perturbation amplitude is $A_3 = 5\%$ and pulse with $P_{max} = 1.5 \times 10^9 Pa$.

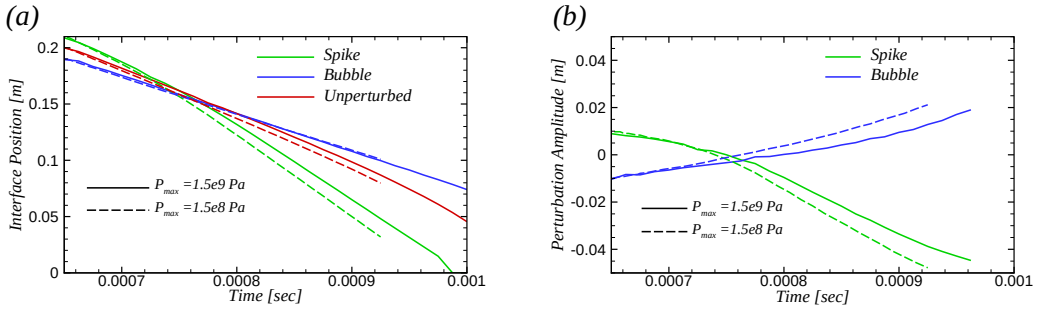

Figure 12: Effect of the pressure pulse amplitude: (a) Radial location of spikes and bubbles (green and blue lines) along with interface location for the unperturbed case (red line). (b) Perturbation amplitude (spikes and bubbles) relative to the unperturbed case. Perturbation amplitude is $A_3 = 5\%$ and azimuthal wave-number is $n = 6$.

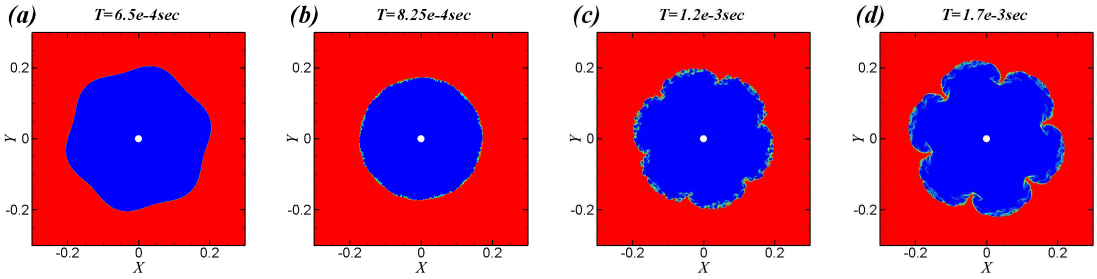

Figure 13: Perturbation evolution for implosion of a molten lead (blue) into water (red). Results are shown by the VoF contours for the perturbation with $A_3 = 5\%$, azimuthal mode number of $n = 6$ and pressure pulse with $P_{max} = 1.5 \times 10^9 Pa$.